Artificial Neural Control of 3-Phase Induction Motor Slip Regulation Using SPWM Voltage Source Inverter

Fadhil A. Hassan* & Lina J. Rashad*

Received on: 27/4 /2009
Accepted on: 11/3/2010

Abstract

Variable-Voltage Variable-Frequency control represents the most successful used method in speed control of 3-phase induction motor, which is implemented by using PWM techniques. This paper proposes modeling and simulation of sinusoidal PWM voltage source inverter as a VVVF A.C drive. The dynamic model, simulation of 3-phase induction motor, and open loop speed control system is proposed too. The PI closed loop controller of rotor slip regulation is illustrated as a traditional speed control method, which gives stable operation behavior of motor speed in the constant torque region with settling time =0.5 sec and maximum overshot =20%, but unstable operation in the field weakening regions with steady state error =15%. The Artificial Neural Network (ANN) is going to be the modern type of speed controller.This paper proposes NARMA-L2 (Nonlinear Autoregressive-Moving Average) neural network as an improved Artificial Neural Network technique, and trained as a close loop slip regulation controller, which gives an ideal performance with settling and rise time = 0.18 sec, maximum overshot and steady state error less than 1% in different speed range and constant air gap flux, including the field weakening regions.

Keywords: Sinusoidal PWM, Speed control of induction motor, PI controller, ANN controller, NARMA-L2 controller

السيطرة العصبية الأصطناعية لتنظيم الأنزلاق في محرك حثي ثلاثي الطور بأستخدام عاكس مصدر الجهد لمضمن عرض النبضة الجيبي

الخلاصة

تمثل طريقة تغيير الجهد والتردد من أنجح الطرق المستخدمة في السيطرة على سرعة المحرك الحثي الثلاثي الطور ، والتي تطبق بأستخدام تقنيات التضمين لعرض النبضة. يقدم هذا البحث النموذج والتمثيل لعاكس مصدر الجهد لمضمن عرض النبضة الجيبي كسواقة مغير الجهد والتردد. كما ويقدم أيضاً النموذج والتمثيل للمحرك الحثي الثلاثي الطور مع مسيطر السرعة ذو الحلقة المفتوحة. كما ويقدم المسيطر التناسبي-التكاملي التقليدي كمسيطر الحلقة المغلقة على سرعة الأنزلاق للجزء الدوار في المحرك، والذي قدم أداءً مستقراً في منطقة ثبات العزم حيث كان زمن الوضع 0,5 ثانية وأقصى مدى أطلاق 20% مع أداءً غير مستقراً في مناطق أضعاف المجال مع خطأ في حالة الأستقرار 15%. أن مسيطرات الشبكات العصبية الأصطناعية في

*Electrical & Electronic Engineering Department, University of Technology/ Baghdad

https://doi.org/10.30684/etj.28.12.9
2412-0758/University of Technology-Iraq, Baghdad, Iraq

طريقها لتصبح المسيطرات العصرية، يقدم هذا البحث (NARMA-L2) كتقنية محسنة للشبكات العصبية الاصطناعية والتي تُدرَّب كمسيطر الحلقة المغلقة على تنظيم الأنزلاق، والذي قدم أداءً مثالياً في مدى سرع مختلفة حيث كان زمن الأرتفاع وزمن الوضع يساوي 0,18 ثانية وكان أقصى أطلاق ومقدار الخطأ في حالة الأستقرار أقل من 1% مع أستقرار لقيمة المجال المغناطيسي في الفجوه الهوائية بضمنها المنطقة الضعيفة المجال .

1-Introduction:

Variable speed industrial applications were used D.C. motors as a powerful drives, because of its strong operation characteristics like simple controller and fast response [1], whereas, A.C. motors were considered as a constant speed drive if operated at constant voltage and frequency, except a few special types of variable speed A.C. motors. But in the last two or three decades, an extensive research and development efforts have be seen to use A.C. motor drives technology because of many economical advantages of A.C. motors like: low cost, low inertia, low maintenance, light weight and have no commutation and brushes problems. For these features A.C. drives are replacing D.C. drives and they are used in many industrial and domestic applications [1, 2].

2- Speed Control of Induction Motor:

The main popular used methods of speed control of I.M. are:

1- Variation of applied voltage.
2- Variation of supply frequency.
3- Variation of stator circuit parameters.
4- Variation of rotor circuit parameters.
5- Constant (*V/f*) variation.

The most popular method used in industrial applications is the constant (*V/f*) control [1, 2], in which the applied voltage "*V*" and frequency '*f*" are varied in the same ratio to maintain the air gap flux at its rated value $\varphi = V_m/k\omega = V_m/k'f$ (where: V_m is the induced EMF, "ω" is the speed, "*f*" is the frequency). Since, controlling the induced EMF "V_m" is difficult, the applied voltage "V_{in}" can be controlled to get approximately constant air gap flux. By ignoring the effect of stator resistance the maximum torque with variation voltage and frequency:

$$Tm = \frac{3Vin^2 \propto^2}{2w_s \propto \sqrt{\propto^2 (X_s + X_r)^2}} \quad ...(1)$$

$$= \frac{3V_{in}{}^2}{2w_s (X_S + X_r)} = const. \quad ..(2)$$

Where:

$$\alpha = \frac{V}{V_{rated}} = \frac{f}{f_{rated}} = variation ratio$$

Fig. (1) illustrated the speed torque characteristic of the I.M. at different variation steps (α). From these curves three operation regions can be verified [1, 2]:

i- Field weakening region-1:

Unfortunately, the effect of stator resistance at low speed region (0%→20% of rated speed) can not be neglected, because of the high percentage voltage drop reduces the induced EMF, flux and torque (dotted curve in fig.1). Thus, in this region it's essential to compensate the voltage drop by using additional posting voltage to restore the maximum torque to its rated value [3].

ii- Constant torque region:

This region spreads from (20%→100%) of rated speed in which the air gap flux, stator current,

slip and torque maintain constant at rated values [3].

iii- Field weakening region-2:

In this region the applied voltage be saturated and the variation being only in frequency causing reduction in stator current and air gap flux [3].

3- Variable (*V/f*) Inverter:

The first generation of A.C. drives used square-wave inverters as speed controlled of low- and medium-power I.M., which consists of controllable A.C. to D.C. converter stage, produces variable D.C. link, which is fed to D.C. to A.C. inverter stage to produce variable frequency square-wave output voltage [4]. After developments in power electronic technology and power semiconductors, pulse width modulation (PMW) technology appears, which minimized the size of the inverter and harmonics contained in the output voltage. In PWM the D.C. link kept constant by a front end diodes bridges, where both output voltage and frequency can be controlled within the inverter stage by switched the power semiconductors "on" and "off" at certain period time to generate variable output voltage and frequency. The most commonly PWM techniques are [1, 3]:

1- Sinusoidal PWM.
2- Selected harmonic elimination (SHE) PWM.
3- Hysteresis band current control PWM.
4- Delta modulation.
5- Space vector (SVPWM).

3-1 SPWM Voltage Source Inverter:

Voltage source inverter (VSI) should have a stiff source at the input, that is, its Thevenin impedance ideally is zero. Thus, a large capacitor can be connected at the input if the voltage source is not stiff. Fig. (2) shows a practical (VSI) consist of power bridge devices with three output legs, each consist of two power switches and two freewheeling diodes, the inverter is supplied from D.C. voltage source via LC or C filter. In sinusoidal PWM the three output legs considered as three independent push-pull amplifiers. The gating signals of each push-pull stage generated by comparing a constant level triangle signal of frequency (f_c) called "carrier signal", with 3-phase sinusoidal signals of frequency (f) called "reference signals", which has variable amplitude to get the desired output voltage, this comparison leads to generate a sequence of variable width pulses used to gating each switch in the push-pull stage. Fig. (3) illustrates the principles of SPWM; gating signals, phase voltage, and line voltage [1].

The output phase voltage:

V_{ao} = is the output phase voltage measured to the center of the input D.C. voltage.

V_{an} = is the output phase voltage measured to isolated neutral of three-phase load such as induction motor.

Where:

$$\begin{bmatrix} V_{an} \\ V_{bn} \\ V_{cn} \end{bmatrix} = \frac{1}{3}\begin{bmatrix} 2 & -1 & -1 \\ -1 & 2 & -1 \\ -1 & -1 & 2 \end{bmatrix} \begin{bmatrix} V_{ao} \\ V_{bo} \\ V_{co} \end{bmatrix} \quad \ldots (3)$$

$V_{ao} = 0.5mV_d \sin(\omega t)$+high-frequency (M $\omega_c \pm N\omega$) [1] …… (4)

Where: ω = fundamental frequency; ω_c = carrier frequency; M and N are integers and M+N =odd, m=modulation index is defined as :

$$m = \frac{V_P}{V_T} \qquad \ldots\ldots..(5)$$

Where: V_P = peak of modulating signal, V_T = peak of triangle signal.

At m= 1, the maximum value of fundamental peak = $0.5V_d$ which is 78.54% of the peak fundamental voltage of the square-wave $(2V_d / p)$ which called the linear modulation region. To further increase the amplitude of the output voltage , the amplitude of the modulating signals exceeds the amplitude of the carrier signal which leads to enter into quasi-PWM region called "over modulating region" causing increase in the low order harmonics. Further increasing modulation index tends to obtain square wave at maximum possible output fundamental$(2V_d / p)$ [1].

3-2 SPWM Inverter simulation:

By using MATLAB/SIMULINK PROGRAM, the SPWM inverter can be simulated, firstly generation of the carrier triangle signal and the three modulating signals by using internal timer and the rated frequency (50 Hz) to obtain the angular speed ($\omega_e t$), then multiplying the angular speed and the amplitude of the signal by the frequency command (f^*_{com}) and voltage command (V^*_{com}) respectively. Secondly, compared the two signal sets to generate the switching signals of three switches used as three push-pull devices. The output of the switches gives (V_{ao}, V_{bo}, V_{co}) then the three phase to load neutral (V_{an}, V_{bn}, V_{cn}) can be achieved by implementing equation (1). Fig. (4) illustrated the complete simulation of SPWM inverter, and the output phase voltage can be shown in fig. (5) for linear modulation region and over modulation region.

4- Modeling and Simulation of 3-phase I.M. :

The mathematical representation of an induction motor can be looked on as transformer with moving secondary winding, where the coupling coefficients between the stator and rotor phases change continuously with the change of rotor position [1, 3]. The machine model can be described by differential equation with time varying mutual inductances, but such model tends to be very complex. Therefore, axis transformation is applied to transfer the three phase parameters (voltage, current and flux) to two-axis frame called (dq-axis stationary frame or park transformation). Park transformation is applied to refer the stator variables to a synchronously rotating reference frame fixed in the rotor, by such transformation the stator and rotor parameters rotate in synchronous speed and all simulated variables in the stationary frame appear as d.c. quantities in the synchronously rotating reference frame [1, 3].

The per-phase equivalent circuit diagram of an I.M. in two- axis synchronously rotating reference frame are illustrated in fig. (6). From the circuit diagram the following equations can be written [1]:

- Stator equation:

$$V_{qs}^{\ e} = R_s i_{qs}^{\ e} + \frac{d\Psi_{qs}}{dt} + w_e \Psi_{ds} \quad \text{.....(6)}$$

$$V_{ds}^{\ e} = R_s i_{ds}^{\ e} + \frac{d\Psi_{ds}}{dt} - w_e \Psi_{qs} \quad \text{.....(7)}$$

● Rotor equation:

$$V_{qr}^{\ e} = R_r i_{qr}^{\ e} + \frac{d\Psi_{qr}}{dt} + (w_e - w_r)\Psi_{dr} \quad ...(8)$$

$$V_{dr}^{\ e} = R_r i_{dr}^{\ e} + \frac{d\Psi_{dr}}{dt} - (w_e - w_r)\Psi_{qr} \quad ....(9)$$

It's obviously that in squirrel cage I.M $V_{qdr}=0$, then the pervious equation can be

rewritten:

$$\frac{d\Psi_{qs}}{dt} = V_{qs}^{\ e} - R_s i_{qs}^{\ e} - w_e \Psi_{ds} ....(10)$$

$$\frac{d\Psi_{ds}^{\ e}}{dt} = V_{ds}^{\ e} - R_s i_{ds}^{\ e} + w_e \Psi_{qs} ....(11)$$

$$\frac{d\Psi_{qr}}{dt} = -R_r i_{qr}^{\ e} - (w_e - w_r)\Psi_{dr} ....(12)$$

$$\frac{d\Psi_{dr}}{dt} = -R_r i_{dr}^{\ e} + (w_e - w_r)\Psi_{qr} ....(13)$$

The development torque by interaction of air gap flux and rotor current can be found as:

$T_e=(3/2)(P/2)\overline{\Psi_m} X \overline{I_r}$ ……..(14)

By resolving the variables into d-q^e components:

$T_e=(3/2)(P/2)(\Psi_{ds} i_{qs}^{\ e} - \Psi_{qs} i_{ds}^{\ e})$ …..(15)

The dynamic torque equation of the rotor:

$$T_e = T_L + (\frac{2}{P}) J \frac{dw_r}{dt} \quad .....(16)$$

Where: ω_r = is the electrical rotor speed; P: no. of poles; J= rotor inertia; T_L= load torque.

The stator current can be found by:

$$i_{qs}^{\ e} = \frac{\Psi_{qs} - \Psi_{dm}}{L_s} \quad .....(17)$$

$$i_{ds}^{\ e} = \frac{\Psi_{ds} - \Psi_{qm}}{L_s} \quad .....(18)$$

The air gap flux :

$$\Psi_{qm} = \frac{L_{m1}}{L_s}\Psi_{qs} + \frac{L_{m1}}{L_r}\Psi_{qr} \quad .....(19)$$

$$\Psi_{dm} = \frac{L_{m1}}{L_s}\Psi_{ds} + \frac{L_{m1}}{L_r}\Psi_{dr} \quad .....(20)$$

Where:

$$L_{m1} = \frac{1}{(\frac{1}{L_m} + \frac{1}{L_s} + \frac{1}{L_r})} ...(21)$$

From the pervious equations the dynamic model of an induction motor is simulated as shown in fig. (7).

5- Open Loop I.M. Drive:

The open loop volt/H_z control of an induction motor is the most popular method of speed control because of its simplicity. This type of A.C. drive consists of variable-voltage variable-frequency inverter such as SPWM inverter, which is connected directly to an induction motor. The speed command signal (ω_e^*) controls both voltage and frequency without any feedback signal or monitoring to the motor quantities like current, speed, torque or flux. As the frequency becomes small at low speed, the stator resistance tends to absorb the major amount of the stator voltage thus weakening the flux, a boost voltage (V_o) is added so that the rated flux, and corresponding full-load torque become available down to zero speed [1]. Fig. (8) Illustrates the overall

open loop system simulation which couples the SPWM model with the I.M. model. The used squirrel cage induction motor name plate is:
3-ph I.M, 380 v., 2.2 kw, 2 poles, 50 Hz, L_s= 13.6 mH, L_r= 11.4 mH, R_s=2.3 Ω, R_r= 3.4 Ω, rotor inertia= $4.5*10^{-3}$ kg/m^2.
The operation performance for different speed commands at full-load is shown in fig. (11). By studying the behavior of the motor speed, torque and flux the following notes can be recorded:

- The rotor speed at full-load less the commands speed for different speed commands by small slip (w_{sl}) which increases in the field weakening regions.
- The air gap flux varies with speed variation, which causes reduction in operation torque.

Therefore, to improve system performance and get exact operating speed with constant air gap flux, close loop control must be implemented [4].

6- PI controller with Slip Regulation:

The closed loop control of A.C. drives is some what complex, and the complexity increases if high performance is demanded. There are wide studies and researches concern with several types of I.M. speed control. The main control techniques including scalar control, vector or field oriented control, direct torque and flux control, adaptive control, and intelligent control. The simplest and popular used method is scalar slip regulation of rotor speed, in which the actual rotor speed measured by means of tacho-meter [2, 4]. The difference between the command speed (w_e^*) and the actual rotor speed (w_r) gives the slip speed (w_{sl}) which added to the rotor speed through proportional-integral (PI) controller to obtain new speed command fed to the inverter. With step-up speed command the motor accelerates freely with a slip limit that corresponds to the torque limit, and then settles down to steady value. With step-down speed command the drive goes into regenerative or dynamic breaking mode and decelerates with constant negative slip $(-w_{sl})$. The overall PI controller system simulation is illustrated in fig. (9), by trial and error the proportional gain (K_p) and integral gain (K_i) selected as (K_p=1, K_i=2). The operation performance of different speed commands are shown in fig. (12). From these results the following notes can be recorded:

- The rotor speed exceeds the command value in the transient response by big overshoot value approximately equal to (20%).
- The settling time of the rotor speeds until reaches the steady state approximately equal to (0.5 sec.).
- There is a small deviation of air gap flux during speed variation steps, which causes torque fluctuation.

7- Neural Controller with Slip Regulation:

Neural networks have been applied very successfully in the identification and control of dynamic systems [4, 5]. The universal approximation capabilities of the multilayer perception make it a popular choice for modeling nonlinear systems and for implementing general-purpose nonlinear controllers [5].

There are three popular neural network architectures for prediction and control that have been implemented in the Neural Network Toolbox [6]:

•Model Predictive Control.

•NARMA-L2 (or Feedback Linearization) Control.

•Model Reference Control.

NARMA-L2 (Nonlinear Autoregressive-Moving Average) neural controller requires the least computation and it's simply a rearrangement of the neural network plant model, which is trained off-line, in batch form. The only online computation is a forward pass through the neural network controller. The drawback of this method is that the plant must either be in companion form, or be capable of approximation by a companion form model (called NARMA-L2) [6, 7].

In this paper the NARMA-L2 neural controller is chosen to adapt the control signal of the A.C drive. The architecture of the NNC is consist of two neural networks (f-NNC and g-NNC), each of them is consist of two input neurons (command input signal and feedback signal) and one output neuron. The number of hidden layers of each network is seven layers with two input and three output delayed steps. The training of the neural networks can be done by using large number of discrete plant input data involve random speed command steps with random durations, and plant open loop response of these input data. Input and output data sets are used to training the two neural networks (f) and (g), then the output of f-Network subtract from the next speed command to generate predictive error signal which divided by the output of g-Network to obtain final new speed command fed to the plant. The neural network architecture is illustrated in fig.(12) and the overall system simulation is shown in fig. (13). The neural network training doing by using Levenberg-Maquardt Back propagation algorithm, to obtain mean square error (MSE) about $5*10^{-6}$ the training data divided into three gropes: one half of the data for training set, one fourth for validation set and one fourth for the test set. The training data, training procedure and training error (MSE) can be shown in fig. (14). The operation performance of different speed command steps is shown in fig. (15-a), and output performance under load condition is shown in fig. (15-b). And the accuracy performance of the ANN for speed range 0-140% of rated speed is illustrated in fig. (16).

From these results the following notes can be recorded.

- The rotor speed exactly equal to the command speed for different variation steps.
- There is no overshoot occur in the transient response.
- The motor has excellent performance in different step-up and step-down steps, also in the field weakening regions.
- The air gap flux gives an excellent and unexpected performance in different speed variation steps, and it behaves as same as field oriented control or flux control method.

8- Conclusions

In this paper the conclusions of this work is summarized in three steps as following:

1- In open loop (volt/Hz) controller the motor speed, torque and flux is

not exactly equal to the desired values.

2- The performance of the PI controller gives:

- Rise time: 0.05 sec. (good).
- Settling time: 0.5 sec. (poor).
- Maximum overshot: 20% (poor).
- Steady state error: 0% in constant torque regions (very good), and 15% in field weakening regions (poor).
- The value of the air gap flux varies with speed variation steps (poor).

3- Neural Network Controller proposes an excellent performance as follow:

- Rise time: 0.18 sec. (poor).
- settling time: 0.18 sec. (very good).
- Maximum overshot: 0% (very good).
- Steady state error: 0% in constant torque regions (very good), 1% in field weakening regions (good).
- Approximately constant air gap flux in different speed variation steps (good).

Therefore, it can be used successfully instead of complex controller methods like field oriented or flux controller.

9- References:

[1] Bimal K. Bose, " *Modern Power Electronic and AC Drives*", Prentice Hall, 2002.

[2] Muhammed H. Rashid, " *Power Electronics, Circuits, Derives and applications*", Pearson Education Inc. 2004.

[3] Fadhil A. Hassan, "*Modeling And Implementation of SVPWM Driver of 3-Phase Induction Motor*", Ms.c. thesis, University of Technology, Iraq, 2008.

[4] Wang Dazhi, Wang Zhenlei, Gu Shusheng, "*Identification and Control of Induction Motor Using Artificial Neural Network*", IEEE, Page: 751-754, 2005, chine.

[5] Yushaizad Yusof, Abdul Halim Mohd, "*Simulation and Modeling of Stator Flux Estimator for Induction Motor Using Artificial Neural Network Technique*", IEEE, 2003.

[6] Howard Demuth, Mark Beale, "*Neural Network Toolbox*", Copyright 1992-2004 by the Math Work, Inc.

[7] Lina J. Rashad, "*Excitation and Governing Control of A Power Generation Based Intelligent System*", Ms.c. thesis, University of Technology, Iraq, 2008.

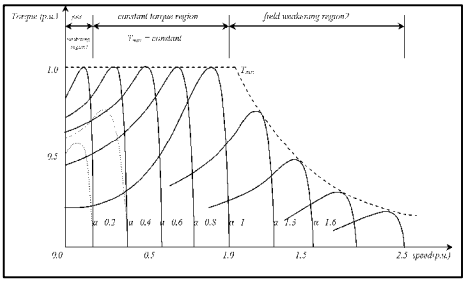

Figure (1) Speed torque characteristic of (V/f) control.

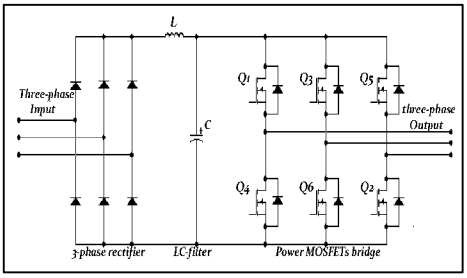

Figure (2) 3-phase voltage source inverter.

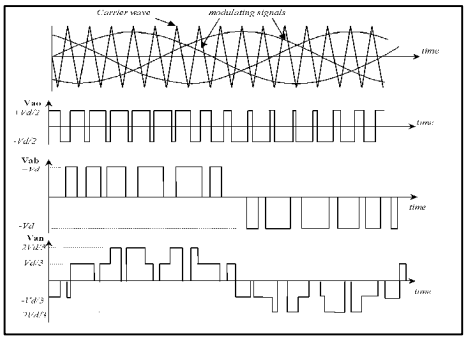

Figure (3) *SPWM principles.*

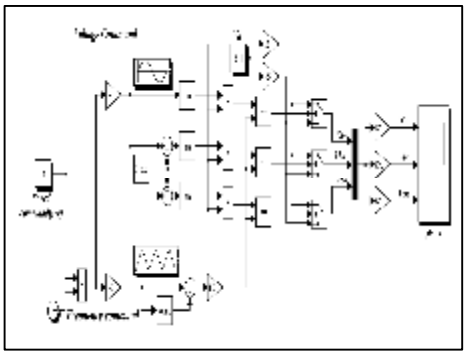

Figure (4) SPWM Simulation.

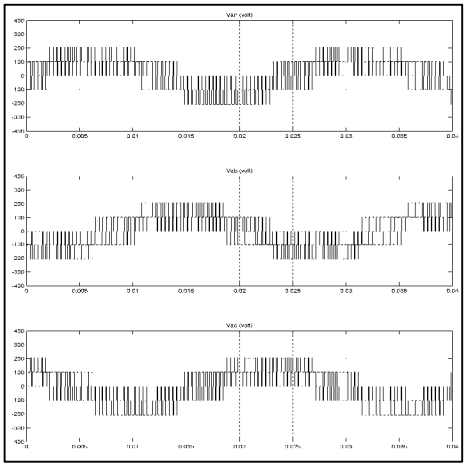

Figure (5) Linear region output phase voltage.

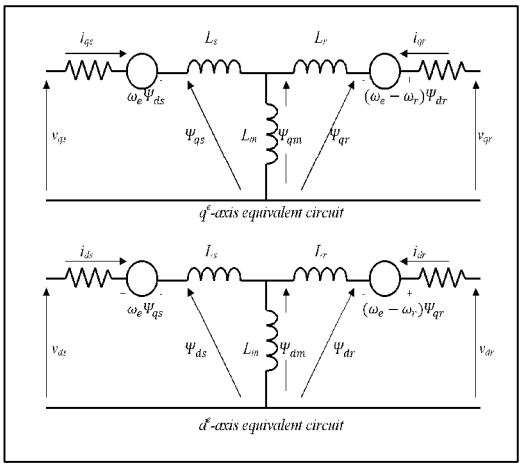

Figure (6) *q^e-d^e I.M equivalent circuit.*

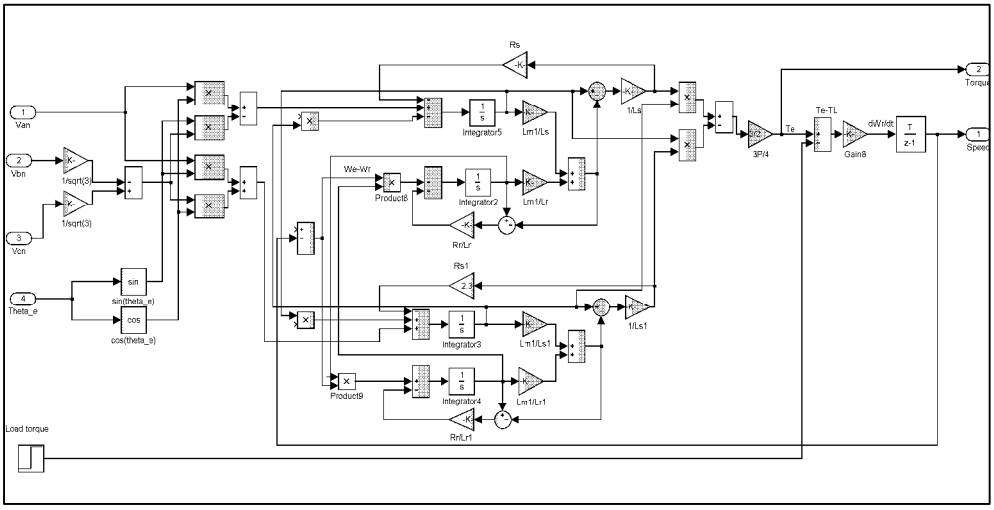

Figure (7) ***I.M simulation.***

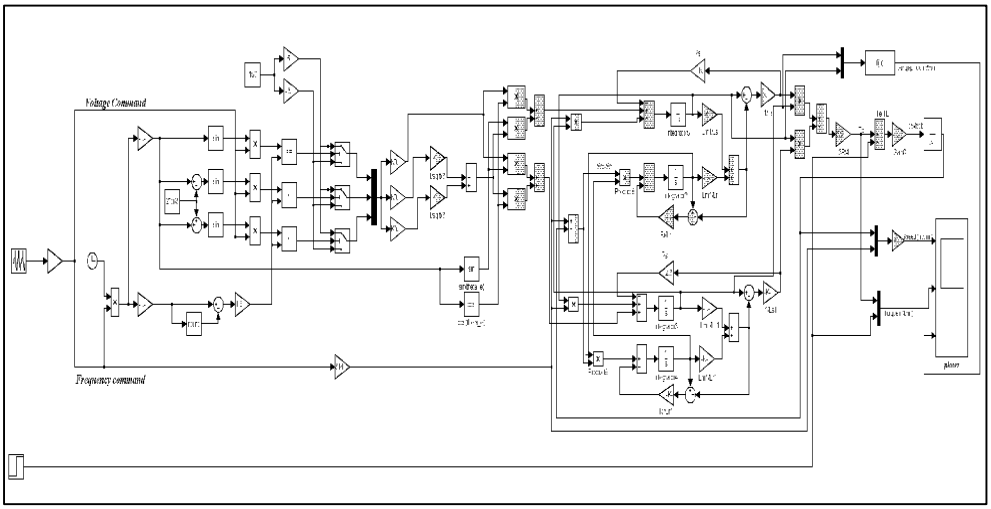

Figure (8) ***Open loop speed control system.***

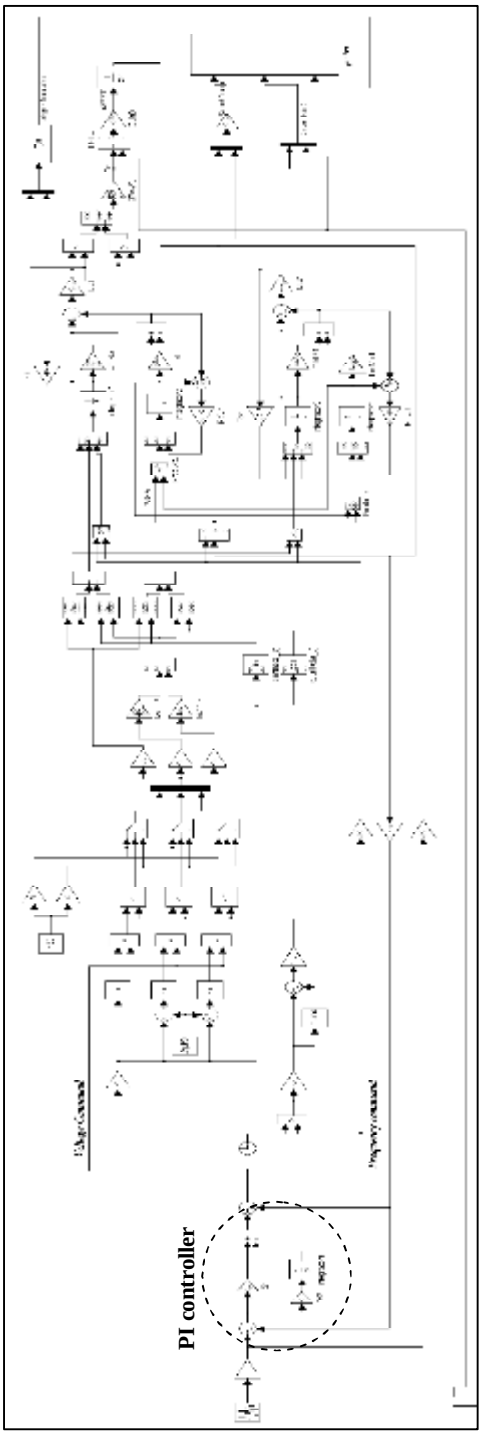

Figure (9) *PI speed controller system*

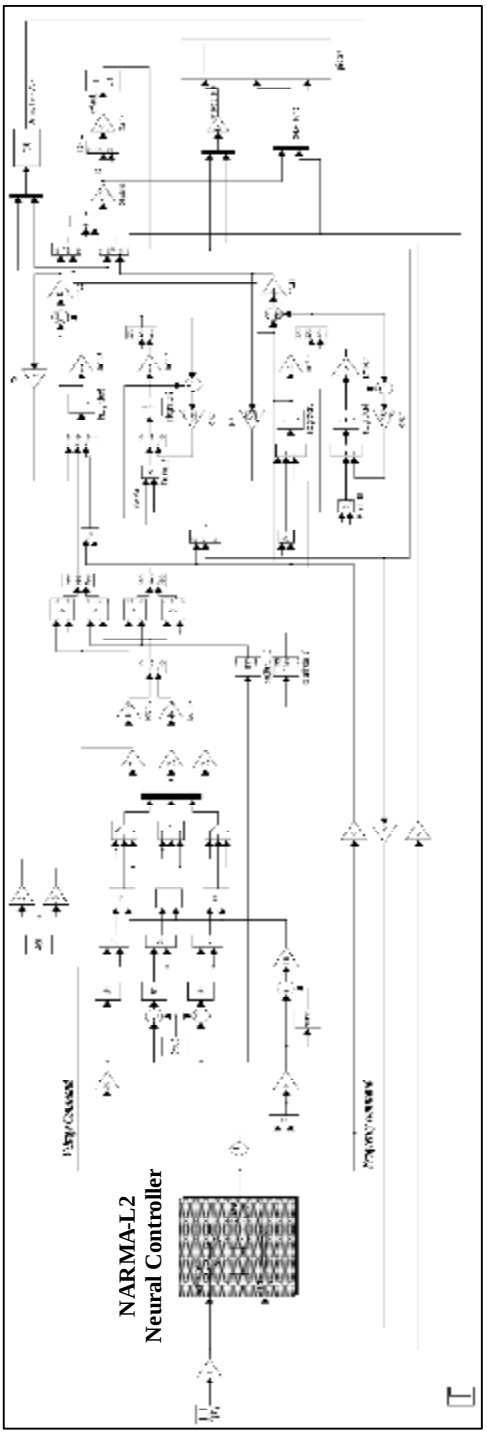

Figure (10) *Neural controller system simulation.*

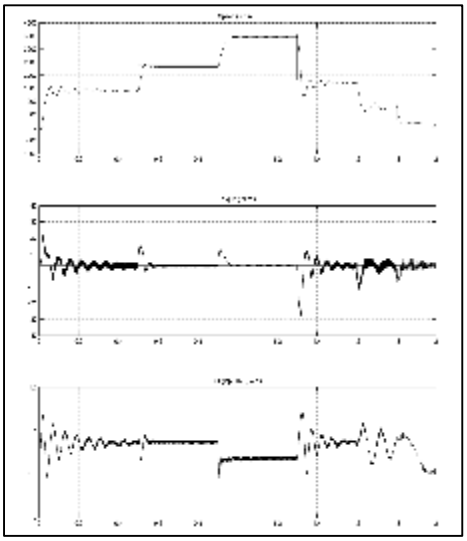

Figure (11) *Open loop performance.*

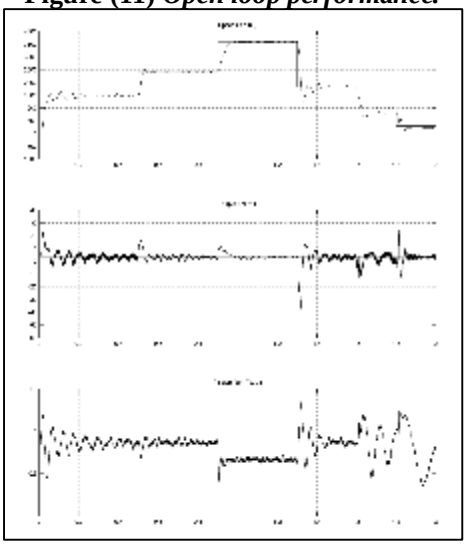

Figure (12) PI control performance.

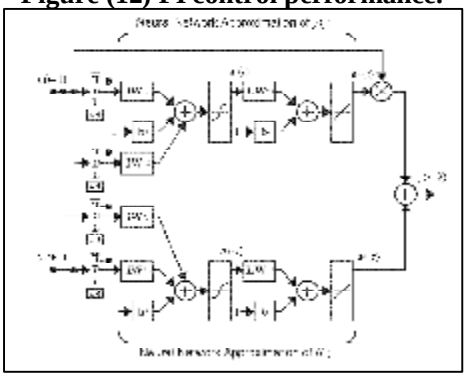

Figure (13) NARMA-L2 architecture.

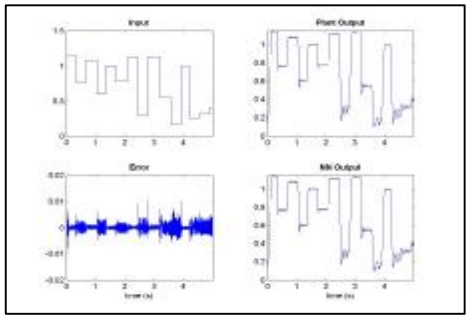

Figure (14-a) *Training data*.

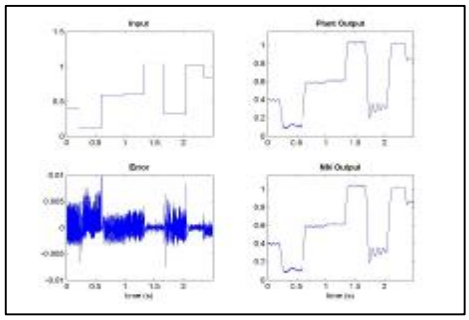

Figure (14-b) Validation data.

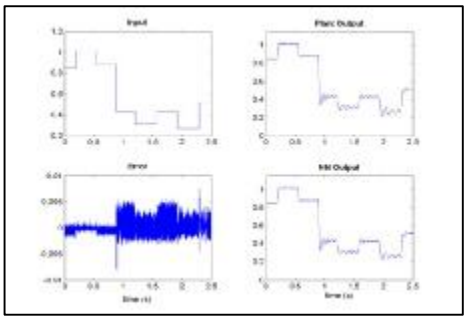

Figure (14-c) Testing data.

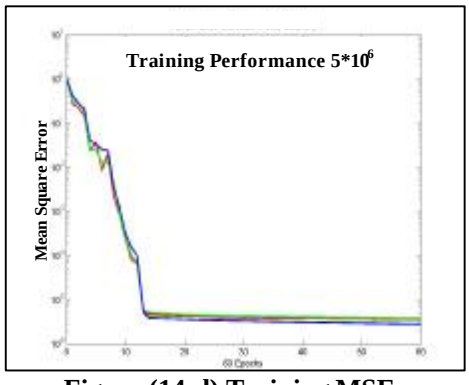

Figure (14-d) Training MSE.

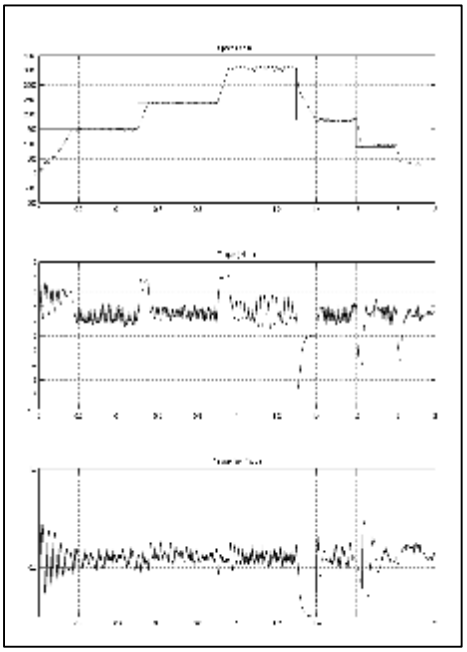

Figure (15-a) Neural control performance.

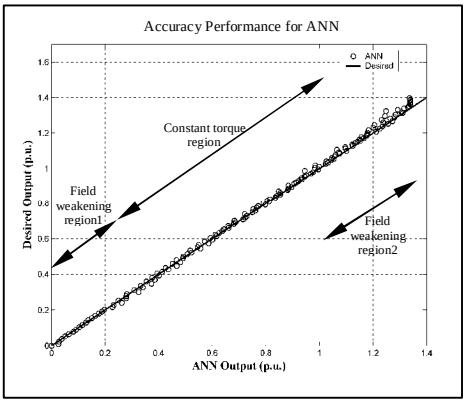

Figure (16) Accuracy performance for ANN.

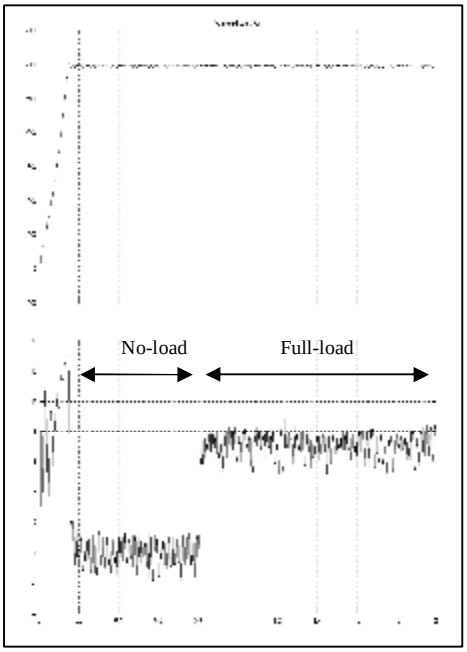

Figure (15-b) Neural performance under load condition.